

## 2D mobile breather scattering in a hexagonal crystal lattice

Jānis Bajārs

*Faculty of Physics, Mathematics and Optometry,  
University of Latvia, Jelgavas Street 3, Riga, LV-1004, Latvia\**

J. Chris Eilbeck

*Maxwell Institute and School of Mathematical & Computer Sciences,  
Heriot-Watt University, Edinburgh, EH14 4AS, United Kingdom†*

Benedict Leimkuhler

*Maxwell Institute and School of Mathematics, The University of Edinburgh,  
James Clerk Maxwell Building, The King's Buildings,  
Mayfield Road, Edinburgh, EH9 3JZ, United Kingdom‡*

(Dated: December 21, 2020)

We describe, for the first time, the full 2D scattering of long-lived breathers in a model hexagonal lattice of atoms. The chosen system, representing an idealized model of mica, combines a Lennard-Jones interatomic potential with an “egg-box” harmonic potential well surface. We investigate the dependence of breather properties on the ratio of the well depths associated to the interaction and on-site potentials. High values of this ratio lead to large spatial displacements in adjacent chains of atoms and thus enhance the two dimensional character of the quasi-one-dimensional breather solutions. This effect is further investigated during breather-breather collisions by following the constrained energy density function in time for a set of randomly excited mobile breather solutions. Certain collisions lead to  $60^\circ$  scattering, and collisions of mobile and stationary breathers can generate a rich variety of states.

The nature of mysterious particle-like tracks in muscovite mica crystals have attracted much recent interest since Russell’s first observations over 50 years ago [1]. Russell suggested that some of them were caused by localized vibrational modes (which he called quodons) in the K-K layer of mica [2, 3]. This hypothesis has led to a number of simulations of breathers in model hexagonal lattices with on-site potentials [4–7]. The surprising conclusion of these studies is that in 2D, localized single breathers can travel along the main crystal directions of the lattice with little attenuation or lateral spreading.

In this note we move beyond the case of single breathers by examining breather-breather collisions. We present evidence that breathers are remarkably robust to collisions, and scattering through some multiple of  $60^\circ$  into another crystal direction is frequently observed in some circumstances. In addition we examine ensembles of initial conditions for breather-breather collisions to begin to understand how the relative angles and phases of the breathers affect their interactions.

Our simplified 2D model of the hexagonal K-K sheet layer in mica crystal [7] is based on the following dimensionless Hamiltonian which describes the classical dy-

namics of  $N$  potassium atoms:

$$H = K_E + U + V_c \quad (1)$$

$$= \sum_{n=1}^N \left( \frac{1}{2} |\dot{\mathbf{r}}_n|^2 + U(\mathbf{r}_n) + \frac{1}{2} \sum_{\substack{n'=1 \\ n' \neq n}}^N V_c(|\mathbf{r}_n - \mathbf{r}_{n'}|) \right),$$

where  $K_E$  is the kinetic energy,  $U$  is the on-site potential energy (modelling forces from atoms above and below the K-K sheet),  $V_c$  is the radial interparticle potential of the potassium atoms with a cut-off radius  $r_c$ ,  $\mathbf{r}_n \in \mathbb{R}^2$  is the 2D position vector of the  $n^{\text{th}}$  K atom,  $\dot{\mathbf{r}}_n$  is its time derivative, and  $|\cdot|$  is the Euclidean distance. Note that no motion in the  $z$ -direction is allowed. Any mention of “transverse” in the following means in-plane motion transverse to the breather propagation line.

The dimensionless on-site potential  $U$  is modelled as a smooth periodic function resembling an egg-box carton with hexagonal symmetry:

$$U(x, y) = \frac{2}{3} \left( 1 - \frac{1}{3} \left( \cos \left( \frac{2\pi(\sqrt{3}x-y)}{\sqrt{3}} \right) + \cos \left( \frac{2\pi(\sqrt{3}x+y)}{\sqrt{3}} \right) + \cos \left( \frac{4\pi y}{\sqrt{3}} \right) \right) \right), \quad (2)$$

where  $x$  and  $y$  are configurational coordinates,  $\mathbf{r}_n = (x, y)$ . Importantly, in any of the three crystallographic lattice directions with direction cosine vectors  $(1, 0)^T$  and  $(1/2, \pm\sqrt{3}/2)^T$ , the on-site potential (2) is a cosine, so the model reduces to a special case of the Frenkel–Kontorova model. The 1D atomic chains in the  $(1, 0)^T$  lattice direction are denoted by  $y_m$ , where  $m \in \mathbb{Z}$ . The

\* Janis.Bajars@lu.lv

† J.C.Eilbeck@hw.ac.uk

‡ B.Leimkuhler@ed.ac.uk

interatomic interactions of K atoms are modelled by a scaled Lennard-Jones potential  $V_{LJ}(r)$  with cut-off radius  $r_c$ , i.e.

$$V_c(r) = \epsilon \left( \left( \frac{1}{r} \right)^{12} - 2 \left( \frac{1}{r} \right)^6 \right) + \epsilon \sum_{j=0}^4 A_j \left( \frac{r}{r_c} \right)^{2j}, \quad (3)$$

if  $0 < r \leq r_c$ , and zero elsewhere. The cut-off dimensionless coefficients  $A_j \rightarrow 0$  when  $r_c \rightarrow \infty$  are determined from matching and continuity conditions on  $V_{LJ}$  at well depth  $r = 1$  and the cutoff  $r_c$ , respectively, see [7] for more details.

In this paper we consider  $r_c = 3$  in dimensionless units. In general, we did not observe qualitatively different results for  $r_c \geq \sqrt{3}$ . This can be attributed to the rapid decay of the Lennard-Jones potential (3) for  $r \rightarrow \infty$ .

The dimensionless parameter  $\epsilon$  controls the relative strength of the two potentials. If  $\epsilon = 0$  then the system decouples into nonlinear oscillators whereas, for  $\epsilon \rightarrow \infty$ , the system behaves as a Lennard-Jones fluid. Previous studies [4] suggest that propagating breather solutions are observed when the two potentials are of roughly equal relative strength. This occurs at about  $\epsilon = 0.05$  [7]. The same paper describes how mobile breather solutions for (1) can be observed in the range  $\epsilon \in [0.001, 1]$ .

We mention here that other studies of hexagonal lattices have mostly concentrated on Morse lattices *without* an on-site potential, see for example [8, 9] and references therein. Ref. [9] discusses general cases of crowdions, also known as kinks, pulses which asymptote to different values in different directions. Ref. [8] discusses solitons collisions with 2D scattering but the scattered pulses are not long-lived. Breather collisions are discussed in [10], but no cases involving  $60^\circ$  are described.

To excite mobile discrete breathers, the simplest method is to consider atoms in their dynamical equilibrium state, i.e. at the bottom of each well of the on-site potential (2), and excite three co-linear neighbouring atomic momenta in any crystallographic lattice direction with the pattern

$$\mathbf{v}_0 = \gamma(-1, 2, -1)^T, \quad (4)$$

where the values of  $\gamma \in \mathbb{R}$  depend on the choice of  $\epsilon$ . In contrast to other initial excitations such as single kicks or more complex patterns, we find that this pattern produces clean initial conditions for the excitation of mobile discrete breather solutions, i.e. produced very few phonons. Note that although this initial pattern appears to sum to equal and opposite kicks in each direction, the effect is not symmetric due to the nonlinearities involved.

Similarly, by considering patterns involving four co-linear atomic momenta  $\mathbf{w}_0 = \gamma(-1, 2, -2, 1)^T$ , we are able to excite stationary breathers. In the present study we concentrate on breather-breather interactions and therefore avoid the complications that a higher phonon density would bring.

We integrate the Hamiltonian dynamics of the system with the second order time reversible symplectic Verlet

method [11, 12]. In the following, all numerical examples are performed with time step  $\tau = 0.04$  and periodic boundary conditions for different values of  $\epsilon$  and  $\gamma$ . We can define an energy density function at each lattice point by assigning to each atom its kinetic energy and on-site potential values as well as half of the interaction potential values. For conciseness we refer to this as the “lattice point energy”. To obtain positive values we redefine  $H := H + |\min\{H\}|$  such that  $H \geq 0$ . In all energy density plots we interpolate  $H$  over a square uniform mesh.

The initial excitation (4) leads [7] to highly localized mobile breather solutions propagating on a chain of atoms in a crystallographic lattice direction with large displacements in the  $x$  direction, almost zero displacements in the  $y$ -axis direction and with small displacements in both axis directions on the chains of atoms adjacent to the main chain of atoms. In addition, the observed mobile breathers are optical with internal<sup>1</sup> frequencies above the phonon linear spectrum.

In considering breather collisions, there are three possibilities. The first is inline or head-to-head collisions with two breathers on the same chain but travelling in opposite directions. These were first looked at briefly in [5]. The second occurs when two breathers approach each other along the same lattice vectors but on adjacent parallel chains. The third occurs when two breathers approach along different lattice vectors, i.e. at an angle of a multiple of  $60^\circ$ .

Before proceeding to the study of collisions, we investigate mobile breather lattice point energies and displacement properties depending on the values of the parameters  $\epsilon$  and  $\gamma$ . We consider a periodic rectangular lattice with hexagonal symmetry of  $N_x = 100$  atoms in the  $x$ -axis direction and  $N_y = 16$  atoms in the  $y$ -axis direction placed in a mechanical equilibrium state. We excite atoms by (4) in the  $(1, 0)^T$  crystallographic lattice direction in the middle of the lattice with respect to the  $y$ -axis and integrate in time until the breather has passed 1000 lattice sites, that is, crossed the domain along the  $x$ -axis direction 100 times. The final computational time varies depending on the parameter  $\epsilon$  and  $\gamma$  values. In what follows, the main horizontal chain of atoms where the breather propagates is indicated by  $y_m$ .

In the first study we fix parameter  $\epsilon = 0.05$  and vary the value of  $\gamma$ , see Fig. 1. In Figure 1, we show five numerical results for different values of gamma, i.e.  $\gamma = 0.4, 0.5, 0.6, 0.7, 0.8$ . In Figure 1(a) we plot the number of sites the breather has passed versus time. Results show that breather propagates faster as the value of  $\gamma$  increases. In Figures 1(b)–1(d), we plot the maximal lattice point energy and maximal displacements in the  $x$  and  $y$ -axis directions, indicated by the functions  $\Delta x$  and  $\Delta y$ , respectively, over the computational time of atoms

<sup>1</sup> By “internal” we mean the carrier wave inside the slowly varying envelope of the breather.

on the atomic chains  $y_{m+k}$ , where  $k = 0, 1, 2, 3, 4$ . Due to symmetry considerations, we have omitted from the figures the results in the  $y_{m-k}$  chains and the plots of the minimal displacement values in the  $x$  and  $y$ -axis directions.

Figure 1(b) shows that most of the propagating breather lattice point energy is localized on the main chain  $y_m$  where the breather propagates and increases with the values of  $\gamma$ . Figures 1(c) and 1(d) demonstrate large atomic displacements of the breather solution on the main chain of atoms  $y_m$  in  $x$ -axis direction while there is almost zero displacement in the  $y$ -axis direction. Equivalently to the energy results, Fig. 1(b) shows that displacements in the  $x$ -axis direction on the main chain of atoms increase with larger values of  $\gamma$ . In contrast, there is no strong evidence of increases in displacements in the  $y$ -axis direction on the adjacent chain of atoms  $y_{m+1}$  for larger values of  $\gamma$ , see Fig. 1(d). Notice the scale differences in Figs. 1(c) and 1(d), and that there are non vanishing displacements of atoms in chains  $y_{m+2}$ ,  $y_{m+3}$  and  $y_{m+4}$ . This is due to the presence of low amplitude phonons in the dynamics. Figure 1 strongly demonstrates the quasi-one-dimensional nature of mobile breather solutions of the lattice model (1).

We contrast the numerical results of Fig. 1 with numerical results of Fig. 2, where we have considered numerical simulations of mobile breather solutions for excitation parameter value  $\gamma = 0.5$  and various values of  $\epsilon$ . We consider five values of  $\epsilon$ , that is,  $\epsilon = 0.01, 0.02, 0.03, 0.05, 0.1$ . Figure 2(a) shows that the breather propagates faster with larger value of  $\epsilon$ , while the maximal energy on the main chain of atoms decreases with increasing value of  $\epsilon$ , see Fig. 2(b). The same can be observed in Fig. 2(c) for atomic displacements in the  $x$ -axis direction. On the contrary, for larger values of  $\epsilon$ , displacements in the  $y$ -axis direction increases on adjacent chain of atoms  $y_{m+1}$ , as can be seen in Fig. 2(d). This strongly indicates the increase of the 2D character of mobile breather solutions in the dynamics with larger values of  $\epsilon$ . This transverse spreading is important when discussing breathers colliding on adjacent, parallel tracks. We confirm this observation in the study of breather energy scattering by breather-breather collisions below. In the present paper for conciseness, we consider only the values  $\epsilon = 0.01, 0.05$ .

The observations of mobile breather spectra and properties presented in [7] are demonstrated here with  $\epsilon = 0.05$  and a head-to-head collision shown in Figure 3. Consider a periodic lattice of size  $N_x = 400$  and  $N_y = 32$  of atoms in their equilibrium state and launch two atomic excitations (4) in the middle of the lattice at each ends of chain  $y_m$ . We indicate left and right excitation parameter values by  $\gamma_l$  and  $\gamma_r$ , respectively of opposite signs, to set the breathers on a collision course. We set  $\gamma_l = 0.4$  and  $\gamma_r = -0.5$ , and integrate in time until  $T_{end} = 1200$ . At around  $t = 700$ , the breathers collide and reappear, see Figure 3. As in many soliton/breather collision scenarios, we cannot distinguish between the cases where the breathers pass through each other, or the case where one

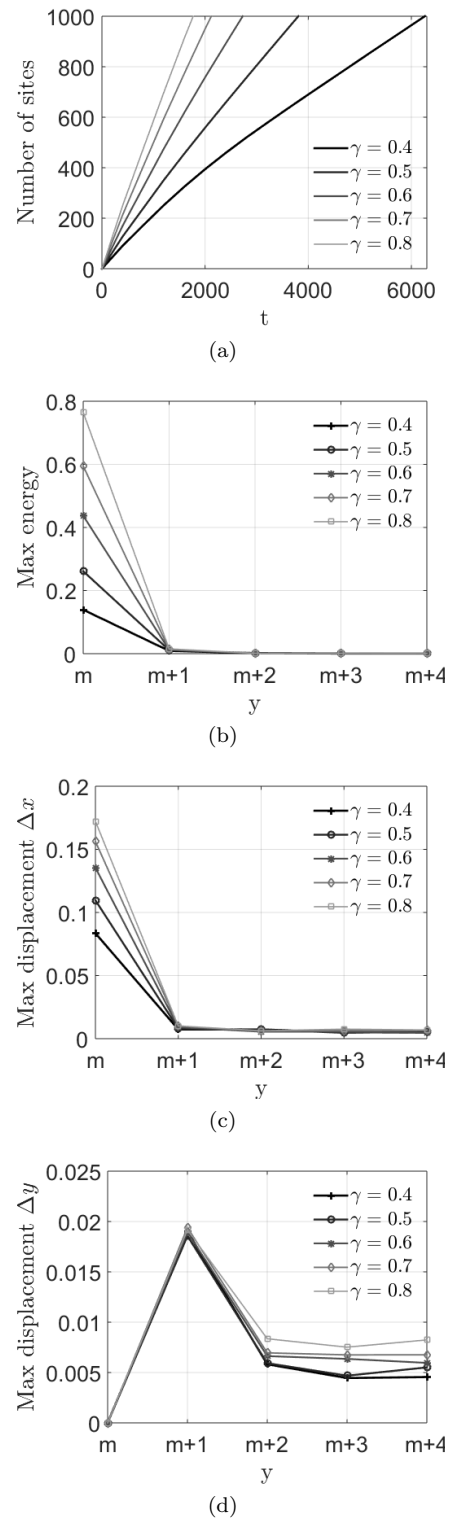


FIG. 1. Mobile breather properties for fixed dimensionless parameter value  $\epsilon = 0.05$  and different values of the excitation parameter  $\gamma$ . (a) breather travel distance versus time in periodic lattice simulation. (b) maximum breather lattice point energy in parallel chains of atoms of propagation. (c) maximal atomic displacements of the breather solutions in the  $x$ -axis direction away from the equilibrium state. (d) maximal atomic displacements of the breather solutions in the  $y$ -axis direction away from the equilibrium state.

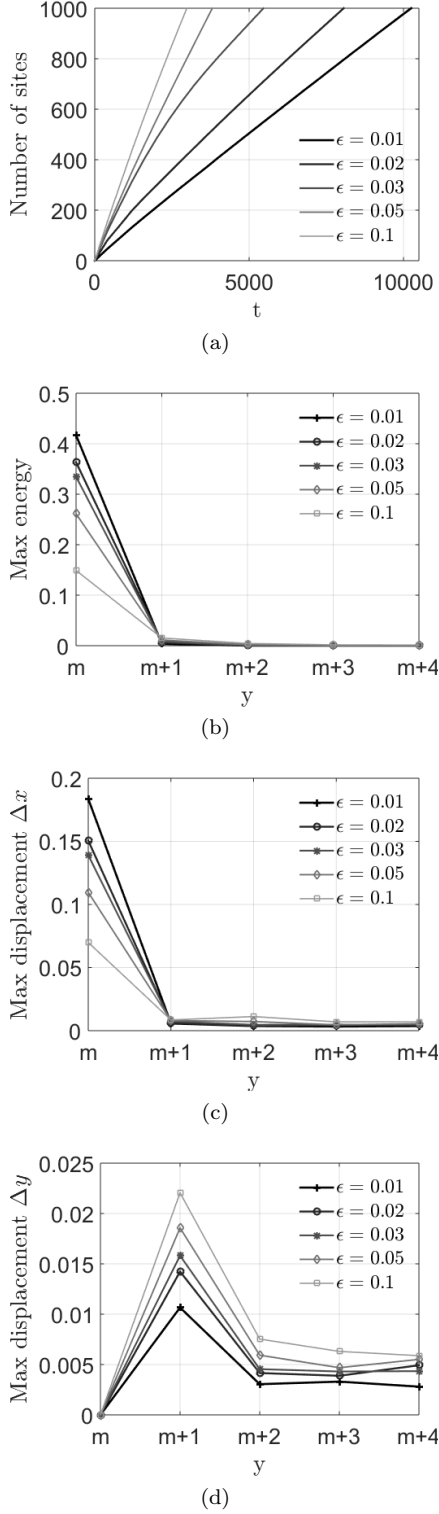


FIG. 2. Mobile breather properties for fixed excitation parameter value  $\gamma = 0.5$  and different values of the dimensionless parameter  $\epsilon$ . (a) breather travel distance versus time in periodic lattice simulation. (b) maximum breather lattice point energy in parallel chains of atoms of propagation. (c) maximal atomic displacements of the breather solutions in the  $x$ -axis direction away from the equilibrium state. (d) maximal atomic displacements of the breather solutions in the  $y$ -axis direction away from the equilibrium state.

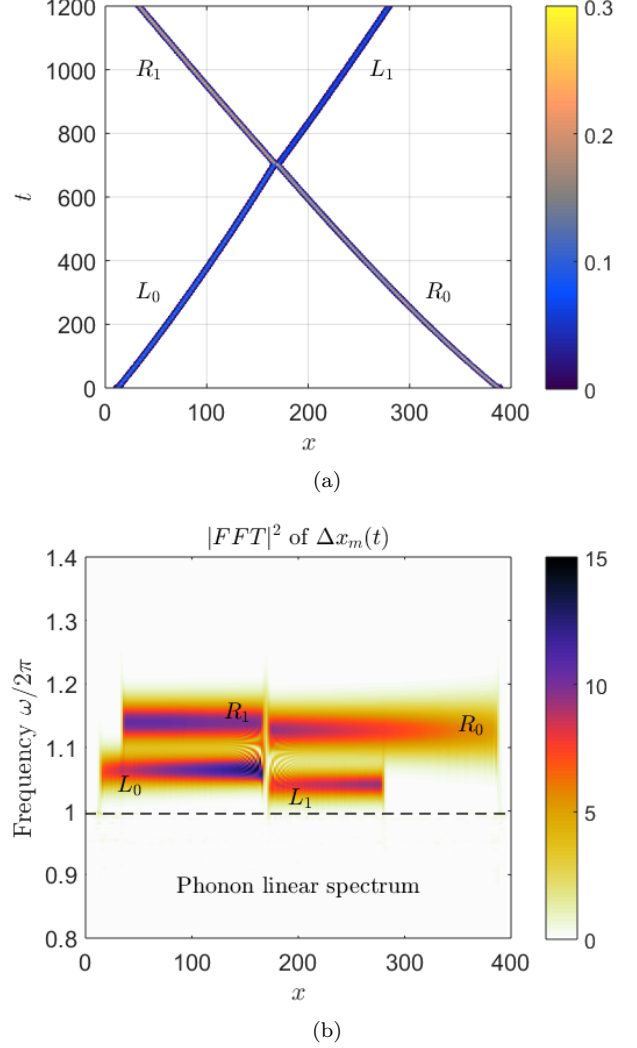


FIG. 3. Simulation of two mobile breather head-to-head collision. (a) lattice point energy function on the main atomic chain of breather propagation. (b) frequency spectrum of atomic displacement function  $\Delta x_m(t)$  in  $x$ -axis direction from equilibrium.

breather bounces off the other without passing through. A more detailed study will be undertaken in future to determine if energy is exchanged or lost in this process.

In Figure 3(a) we plot the lattice point energy function in time of the atoms on the main chain  $y_m$  where the greatest energy of the breather solution is localized. We indicate by  $L_0$  and  $R_0$  the left and right propagating breathers before collision, respectively, while by  $L_1$  and  $R_1$  we indicate the same breathers after the collision. Notice the slight change in the breather propagation speed after the collision. The frequency spectrum is seen in Fig. 3(b), where we use the same notation to identify breather solutions. Note also the breather frequency focusing in time before and after the collision, as was observed in [7]. In addition to breather atomic dis-

placement spectrum we have identified the phonon linear spectrum band of the dispersion relation calculated in [7].

The result of Figure 3 can be thought of as demonstrating a strongly one-dimensional nature, despite the 2D nature of the lattice. Due to the chaotic nature of molecular dynamics, the numerical observations, particularly at long times, are sensitive to changes in the initial conditions and to round-off error. This motivates us to consider an ensemble of initial conditions as well as different starting configurations, to study breather-breather collisions.

For the ensemble, we draw two sets of normally distributed random numbers  $X, Y \sim \mathcal{N}(0, 1)$  and scale them to normally distributed numbers with mean values  $\gamma_{l,r}$  and variance  $\sigma_{l,r}^2$ . Thus we obtain two sets of the excitation parameter value  $\gamma \sim \mathcal{N}(\gamma_{l,r}, \sigma_{l,r}^2)$  for numerical simulations. For the following examples on the lattice  $N_x = 200$  and  $N_y = 64$ , we consider two sets of 2000 random numbers sampling the standard Cauchy distribution (i.e. of the ratio  $X/Y$ ) and scale parameters equal to zero and one, respectively, with mean values  $\gamma_{l,r} = \pm 0.5$  and variances  $\sigma_{l,r}^2 = 0.002$ . Since a small amount of energy is present in the lattice, from phonons generated from the initial excitations, we set atomic energy density values to zero if the value is smaller than 0.01. This value is estimated from the numerical observations. Thus most of the phonon energy is disregarded for the final energy averages and most of the information comes from the breather solutions.

Using this set of initial velocities for *inline* collisions (as in Fig. 3) we did not observe scattering of breather solutions into different crystallographic lattice directions despite a visible spread of energy around the main chain of atoms of breather propagation. Despite that, depending on the  $\gamma_l$  and  $\gamma_r$  values, we observed rich collision events such as the appearance of just one moving or stationary breather, two breathers moving in the same direction and one stationary breather together with one moving breather. Predominantly, the most common case of all was the appearance of two moving breathers after a collision.

If instead we consider the scattering of two breathers on *adjacent* parallel lines, the results depend on the value of  $\epsilon$  used. For  $\epsilon = 0.01$ , Fig. 4(a), we observed no scattering of breather solutions into different crystallographic lattice directions. However for  $\epsilon = 0.05$ , we observe breather scattering in all lattice directions, Fig. 4(b). Notice that dark energy lines arise *only* in these directions indicating propagating as well as stationary breather solutions. Collisions may even lead to fast moving breathers which due to periodic boundary conditions enter back into the computational domain.

To better illustrate breather 2D scattering in Fig. 4(b) we consider a single collision with excitation parameter values:  $\gamma_l = 0.475$  and  $\gamma_r = -0.57$ . In Figure 5 we plot the energy density function at four different times. At time  $t = 120$ , Fig. 5(a), two breathers are moving

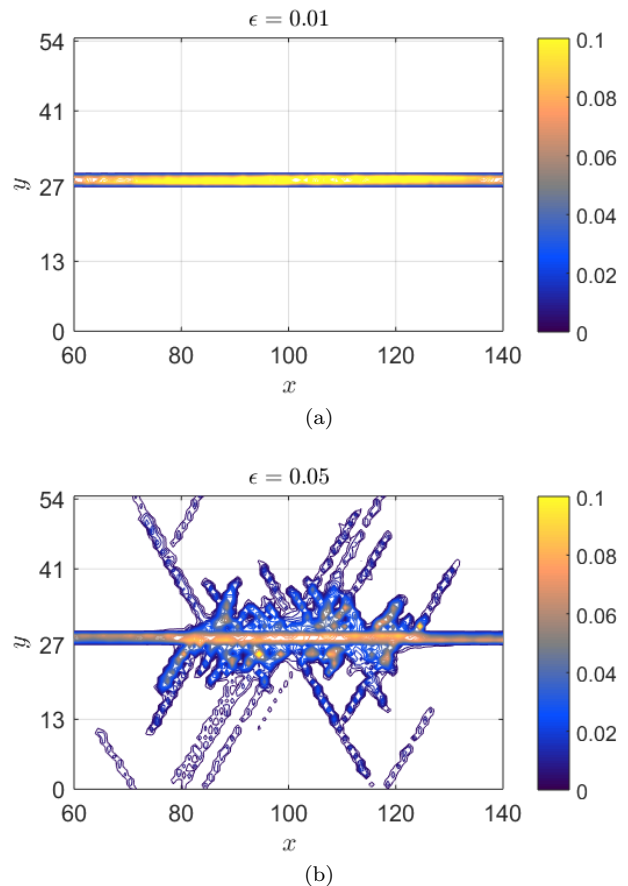


FIG. 4. Constrained ( $H > 0.01$ ) energy density function averaged over 50 time snapshots and 2000 individual simulations of breather-breather collisions on adjacent chains of atoms. (a) simulation with  $\epsilon = 0.01$  until  $T_{end} = 1000$ . (b) simulation with  $\epsilon = 0.05$  until  $T_{end} = 500$ .

towards each other. Around time  $t = 160$ , Fig. 5(b), both breathers collide. The mobile breather from the right continues its path after the collision, while the moving breather from the left gets scattered with an angle, see Figures 5(c) and 5(d).

These examples demonstrate the 2D properties of breather solutions, energy scattering by breathers and the importance of the parameter  $\epsilon$ . Figure 4(b) confirms that the mobile breather's 2D character increases for larger values of  $\epsilon$ , that is, for a stronger interaction potential relative to a weaker on-site potential energy. Since the Hamiltonian (1) is time reversible, Fig. 4(b) also demonstrates breather-breather collisions with an angle to each other when the time is reversed.

To explore further breather scattering by breather-breather collisions in 2D lattice model (1) we consider simulations of mobile breather collisions with a *stationary* breather at an angle to the incoming in Fig. 6. We consider four different locations of the  $(1, -2, 2, -1)$  stationary excitation pattern indicated by black circles while mobile breather propagation directions are indicated by

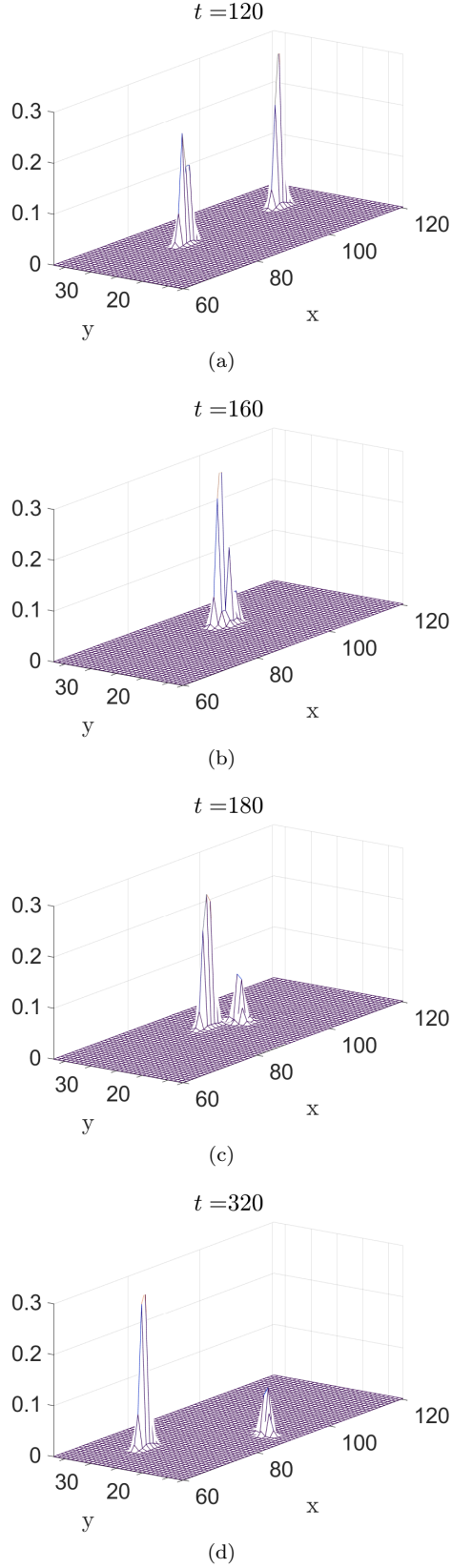


FIG. 5. Lattice point energy density function of a single moving breather collision on adjacent parallel lines at four different times. (a)  $t = 120$ . (b)  $t = 160$ . (c)  $t = 180$ . (d)  $t = 320$ . Parameter values:  $\epsilon = 0.05$ ,  $\gamma_l = 0.475$  and  $\gamma_r = -0.57$ .

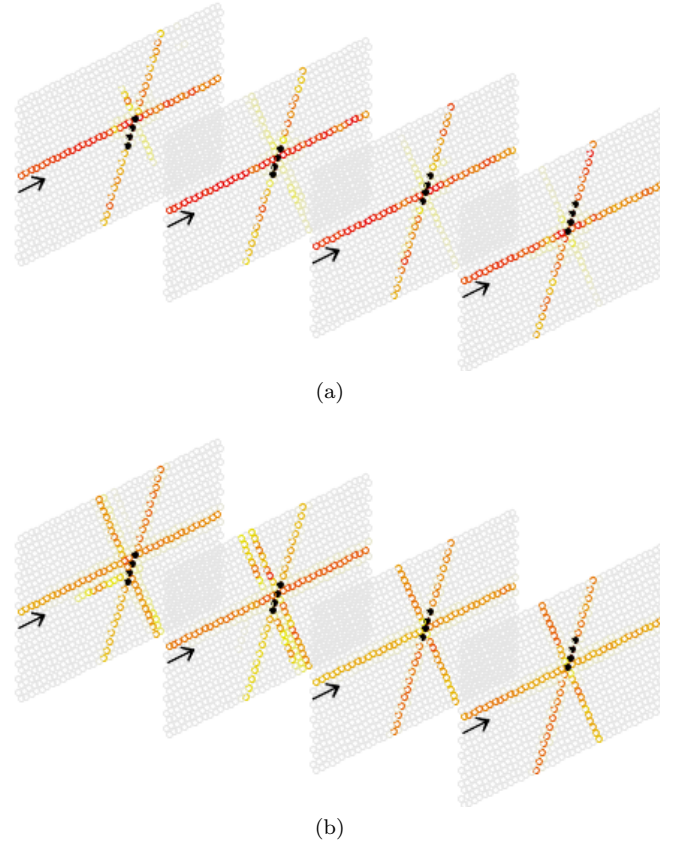


FIG. 6. Constrained ( $H > 0.01$ ) energy density function averaged over 50 time snapshots and 2000 individual simulations of mobile breather collisions with a stationary breather on a crystal axis at  $60^\circ$  to the moving one. The stationary breather is at slightly different positions in each case. (a) simulation with  $\epsilon = 0.01$  until  $T_{end} = 1000$ . (b) simulation with  $\epsilon = 0.05$  until  $T_{end} = 500$ .

black arrows.

For this experiment we consider a smaller size lattice,  $N_x = 120$  and  $N_y = 64$ , and integrate until  $T_{end} = 500$ , if  $\epsilon = 0.05$ , and until  $T_{end} = 1000$ , if  $\epsilon = 0.01$ . We consider a mean excitation value of  $\gamma_l = 0.5$  and  $\gamma_r = -0.35$  where  $\gamma_r$  refers to the stationary breather and variances  $\sigma_l^2 = 0.001$  and  $\sigma_r^2 = 0.00025$ . We used a much smaller variance value for the stationary breather compared to the moving one to ensure that the excitation is not too large to generate a mobile breather.

Because of the spread in incoming velocities/strengths etc., the relative *phases* of the two breathers will also be different in each simulation.

As above, we observe stronger breather scattering in the computations with  $\epsilon = 0.05$ , Fig. 6(b), in contrast to the simulations with  $\epsilon = 0.01$ , Fig. 6(a), where the scattering is predominately only in the lattice directions of both breathers.

Not only do we see scattering through a multiple of  $60^\circ$ , but the details of which track the breathers scatters to is very sensitive to the velocity and phase of the

incoming breather as well as the position of the stationary breather. To better interpret the results of Figure 6 we note that the energy plot illustrates a rich variety of states, e.g., single stationary or moving breathers in all lattice directions, two breathers moving with an angle to each other and two breathers of which one is stationary.

Our study has given us a better understanding of particle-like tracks in muscovite mica crystals. We demonstrate the importance of the relative strengths of the interatomic force and of the force from the surrounding atoms for the existence of long-lived propagating breathers and their 2D collision properties. Recent experimental work by Russell et al. [13] suggests strongly that breather-like objects are important in real 3D crys-

tals of several different materials, displaying hyperconductivity and annealing effects at finite temperatures despite a range of defects such as impurities, dislocations, and crystal boundaries. We plan to extend the current model to one covering more realistic physical situations.

JB, during his postdoctoral research at the University of Edinburgh, and BJL acknowledge the support of the Engineering and Physical Sciences Research Council which has funded this work as part of the Numerical Algorithms and Intelligent Software Centre under Grant EP/G036136/1. JCE thanks Mike Russell for many useful conversations. We are most grateful to an anonymous referee for many helpful comments and corrections.

- 
- [1] F. M. Russell. Tracks in mica caused by electron showers. *Nature*, 216:907, 1967.
  - [2] F. M. Russell. Decorated track recording mechanisms in Muscovite mica. *Nucl. Tracks Radia. Meas.*, 19:109–113, 1991.
  - [3] F. Michael Russell, Juan F. R. Archilla, and Santiago Medina-Carrasco. Localized waves in silicates. What we know from experiments? *arXiv e-prints*, page arXiv:2011.07936, November 2020.
  - [4] J. L. Marín, J. C. Eilbeck, and F. M. Russell. Localized moving breathers in a 2D hexagonal lattice. *Physics Letters A*, 248:225–229, 1998.
  - [5] J. L. Marín, J. C. Eilbeck, and F. M. Russell. 2-D Breathers and applications. In P. L. Christiansen et al., editors, *Nonlinear Science at the Dawn of the 21th Century*, pages 293–306. Springer, Berlin, 2000.
  - [6] J. Bajars, J. C. Eilbeck, and B. Leimkuhler. Numerical simulations of nonlinear modes in mica: past, present and future. In [14], pages 35–67, 2015.
  - [7] J. Bajars, J. C. Eilbeck, and B. Leimkuhler. Nonlinear propagating localized modes in a 2D hexagonal crystal lattice. *Physica D: Nonlinear Phenomena*, 301:8–20, 2015.
  - [8] A. Chetverikov, W. Ebeling, and M. G. Velarde. Collisions of quasi-one-dimensional solitons in triangular Morse lattice. *Letters on materials*, 6:82–85, 2016.
  - [9] I. A. Shepelev, E. A. Korznikova, D. V. Bachurin, A. S. Semenov, A. P. Chetverikov, and S. V. Dmitriev. Supersonic crowdion clusters in 2D Morse lattice. *Physics Letters A*, 384:126032, 2020.
  - [10] A. A. Kistanov, V. D. Sergey, A. P. Chetverikov, and M. G. Velarde. Head-on and head-off collisions of discrete breathers in two-dimensional anharmonic crystal lattices. *Eur. Phys. J. B*, 87:211, 2014.
  - [11] M. P. Allen and D. J. Tildesley. *Computer Simulation of Liquids*. Oxford science publications. OUP, USA, 1989.
  - [12] Benedict Leimkuhler and Sebastian Reich. *Simulating Hamiltonian Dynamics*. Cambridge University Press, 2005.
  - [13] F. M. Russell, M. W. Russell, and J. F. R. Archilla. Hyperconductivity in fluorphlogopite at 300K and 1.1 T. *EPL*, 127:16001, 2019.
  - [14] J. F. R. Archilla et al., editors. *Quodons in mica: nonlinear localized travelling excitations in crystals*, volume 221 of *Springer Series in Materials Science*. Springer International Publishing, 2015.